JOURNAL OF Materials CHEMISTRY

Synthesis and electrochemical characteristics of spinel phase $LiMn_2O_4$-based cathode materials for lithium polymer batteries

Yang-Kook Sun* and Sung-Ho Jin

Polymer Materials Laboratory, Chemical Sector, Samsung Advanced Institute of Technology, 103-12, Moonji-Dong, Yusong-Gu, Daejon, Korea, 305-380. E-mail: yksun@saitgw.sait.samsung.co.kr

Received 15th June 1998, Accepted 11th August 1998

Spinel $LiMn_2O_4$ and $LiMn_{1.95}Ni_{0.05}O_4$ powders have been synthesized by a sol–gel method using an aqueous solution of metal acetates containing glycine. The dependence of the physicochemical properties of the spinel $LiMn_2O_4$ powders on the calcination temperature and glycine quantity have been extensively investigated. The porous $LiMn_2O_4$ and $LiMn_{1.95}N_{0.05}O_4$ electrodes were electrochemically characterized by using charge/discharge experiments along with ac impedance spectroscopy. The $LiMn_{1.95}Ni_{0.05}O_4$ electrode exhibited improved cycling performance in comparison with the stoichiometric $LiMn_2O_4$ one in spite of a small reduction in the initial capacity. The good capacity retention of the $LiMn_{1.95}Ni_{0.05}O_4$ electrode is attributed to stabilization of the spinel structure by Ni doping for Mn ion sites and higher chemical diffusivity of lithium ions with cycling.

Introduction

The spinel $LiMn_2O_4$ has been extensively studied as the most promising cathode material for lithium secondary batteries with high energy density. This material offers several distinct advantages; it is easier to prepare, less expensive and less toxic than layered oxides such as $LiCoO_2$ and $LiNiO_2$.[1,2] However, $LiMn_2O_4$ has problems related to capacity fading and limited cyclability in the 4 V_{Li/Li^+} region in comparison with the layered oxides. The reason for capacity fading has not been clearly resolved, but some possible factors have been proposed.[3–5] In order to improve capacity fading and cyclability of the $LiMn_2O_4$ powders in the 4 V_{Li/Li^+} region, the effects of adding excess lithium to the $LiMn_2O_4$ spinel,[3,6–8] and manganese-substituted spinels $LiM_xMn_{2-x}O_4$ (M = Mg, Zn, Co, Cr, Ni, Al, Ti, Fe, Ga)[3,9–13] have been studied.

The electrochemical properties of $LiMn_2O_4$ strongly depend on its synthetic method. The $LiMn_2O_4$ powders have been usually prepared by solid-state reaction which consists of extensive mechanical mixing and extended grinding, which is detrimental to the quality of the final products. These synthetic conditions can result in inhomogeneity, irregular morphology, larger particle size with broad particle size distribution, and poor control of stoichiometry. In order to achieve good efficiency of Li utilization at high current rates and reliability of lithium secondary batteries, a sol–gel method has been introduced, which is a desirable method to obtain cathode materials with good homogeneity, uniform morphology and narrow size distribution.[14,15] Recently, one of us has reported that the spinel $LiMn_2O_4$ powders being phase pure and having excellent rechargeability could be synthesized by the sol–gel method using glycolic acid and poly(acrylic acid) (PAA) as chelating agents.[8,16]

Lithium polymer batteries are now being studied extensively as promising candidates for electric vehicles and portable electric equipment. The use of a polymer electrolyte would make the batteries highly safe, flexible, light, and thin. One of the problems with the lithium polymer batteries is a progressive capacity fading on repeated cycling. When a polymer electrolyte is used, the establishment of a proper interfacial contact between polymer electrolyte and electrode can be an issue of major concern and essential to guarantee acceptable performance and cycle life. A few studies have been carried out in order to investigate interfacial characteristics between polymer electrolyte and electrode.[17–21]

In this work, $LiMn_2O_4$ and $LiMn_{1.95}Ni_{0.05}O_4$ powders with uniform submicron-sized particles were synthesized by a sol–gel method using glycine as a chelating agent at considerably lower temperatures and shorter times compared with solid-state reaction. Also, the origin of capacity fading on cycling was investigated in terms of interfacial characteristics by using charge/discharge experiments complementary with ac impedance measurements for Li/polymer electrolyte/$LiMn_2O_4$ and $LiMn_{1.95}Ni_{0.05}O_4$ cells.

Experimental

A stoichiometric amount of Li, Mn, and Ni acetates (Acros Co., high purity) with the cationic ratio Li : Mn = 1 : 2 or Li : Mn : Ni = 1 : 1.95 : 0.05 were dissolved in doubly distilled water, mixed well with each other and an aqueous solution of glycine was added (Aldrich, high purity). Glycine was used as a chelating agent to produce gel precursors. Ammonium hydroxide was added slowly to this solution with constant stirring until a pH of 5.0–7.5 was achieved. The resultant solution (0.1 mol aqueous solution of total metal ions) was evaporated at 70–80 °C for 5 h until a transparent sol was obtained. To remove water from the sol the transparent sol was heated at 70–80 °C while being mechanically stirred with a magnetic stirrer. As the evaporation of water proceeded, the sol turned into a viscous transparent gel. For the preparation of the gel precursors with different molar ratios of glycine to total metal ions the same procedure was repeated with the molar ratio of glycine to total metal ions being varied to 1, 1.5, 2, and 2.5 : 1. The gel precursors obtained were decomposed at 250–800 °C for 10 h in air to obtain phase-pure polycrystalline $LiMn_2O_4$ powders.

Powder X-ray diffraction (Rint-2000, Rigaku) using Cu-Kα radiation was used to identify the crystalline phase of the materials calcined at various temperatures. Rietveld refinement was then performed on the X-ray diffraction data to obtain lattice constants. The change in the particle morphology was observed using a field emission scanning electron microscope (TOPCON, ABT-150F).

The electrochemical properties of $LiMn_{2-x}Ni_xO_4$ powders were determined in the Li/polymer electrolyte/$LiMn_{2-x}Ni_xO_4$ cells. The polymer electrolyte was made from polyacrylonitrile (PAN), plasticized by a solution of $LiClO_4$ in a 1 : 1 mixture of ethylene carbonate (EC) and propylene carbonate (PC).

A typical polymer electrolyte composition was PAN 12 wt.%–EC40 wt.%–PC 40 wt.%–$LiClO_4$ 8 wt.%. The ionic conductivity of the polymer electrolyte was $2 \times 10^{-3}\ \Omega^{-1}\ cm^{-1}$ at room temperature. The composite cathode was made from the as-synthesized $LiMn_{2-x}Ni_xO_4$ spinel powders (89.5 wt.%.), acetylene black (Super-P, conducting agent; 5.5 wt.%), and PAN binder (5 wt.%). The $LiMn_{2-x}Ni_xO_4$ spinel powders and acetylene black were added to PAN solution in dimethyl sulfoxide (DMSO) as a solvent. The slurry was spread onto an aluminum foil current collector, and dried at 110 °C in air. Dried composite cathode was then compressed with a roll presser and further dried under vacuum for 10 h at 110 °C. A three-electrode cell was used for the electrochemical measurements. The reference and counter electrodes consisted of 50 μm thick Li foil (Cyprus Foote Mineral Co.) pressed onto a Cu current collector. A rechargeable lithium polymer cell was assembled by sandwiching the polymer electrolyte between the lithium anode and the composite cathode. A lithium electrode contacting polymer electrolytes in proximity to the working electrode served as the reference electrode. The cell was then enclosed in a metallized plastic bag and vacuum sealed. All assemblies of the cell were carried out in a dry box filled with argon gas. The cells were usually cycled between cut-off voltages of 3.4 and 4.3 V_{Li/Li^+} at a constant current density of 0.15 mA cm^{-2}, unless otherwise noted. The cells were activated during the first cycle at a constant current density of 0.1 mA cm^{-2}. ac impedance measurements were performed using a Zahner Elektrik IM6 impedance analyzer over the frequency range of 1 mHz–100 kHz with an amplitude of 5 mV. Each sample was allowed to equilibrate for 30 min at each cycle before measurement at the fully charged state.

Results and discussion

Fig. 1 shows the X-ray diffraction (XRD) patterns of the $LiMn_2O_4$ powders calcined at various temperatures and $LiMn_{1.95}Ni_{0.05}O_4$ powders calcined at 800 °C for 10 h in air, where the molar ratio of glycine to total metal ions was 1.0 : 1. The X-ray diffraction patterns for the powders calcined at 250 °C represent the slow appearance of low crystalline $LiMn_2O_4$ spinel. Impurity peaks corresponding to Li_2CO_3 and $MnCO_3$ are not observed, but are often found in other low temperature techniques. It was confirmed from the XRD patterns that the well-defined spinel $LiMn_2O_4$ phase was formed over the whole calcination temperature range. For all powders, there is no (220) diffraction line ($2\theta = 30.4°$) which is generated by Li ions at 8a sites in the $LiMn_2O_4$ host, because the scattering factor of Li ions is very small. The diffraction

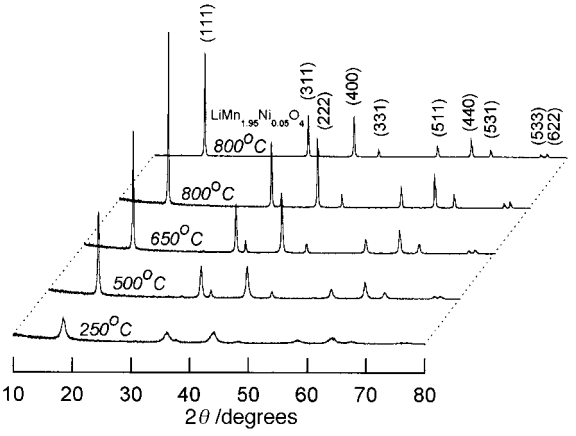

Fig. 1 X-Ray diffraction patterns of the $LiMn_2O_4$ powders calcined at various temperatures and $LiMn_{1.95}Ni_{0.05}O_4$ powders calcined at 800 °C for 10 h in air when the molar ratio of glycine to total metal ions was 1.0 : 1.

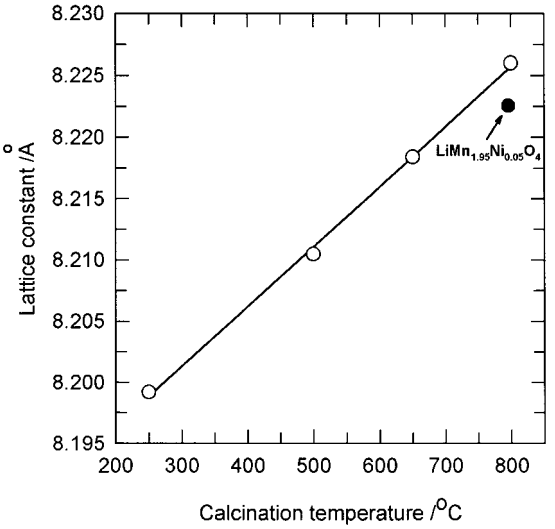

Fig. 2 Effect of the calcination temperature on the lattice constant of the $LiMn_2O_4$ powders (●: $LiMn_{1.95}Ni_{0.05}O_4$ powders calcined at 800 °C) when the molar ratio of glycine to total metal ions was 1.0 : 1.

peaks are much sharper, the widths of the peaks are much narrower, and the positions of the diffraction lines shift to the low angle side in the XRD pattern with the increase of the calcination temperature, which indicates an increase in crystallinity and a gradual growth of average size particles. Similar results had already been reported whereby the $LiMn_2O_4$ powders were synthesized by the sol–gel method using glycolic acid and poly(acrylic acid) as chelating agents.[8,16]

Fig. 2 shows the effect of the calcination temperature on the lattice constant a of the same powders as shown in Fig. 1, obtained from the Rietveld refinement on the XRD data in the cubic unit cell of the $LiMn_2O_4$ powders. It is seen from the figure that the lattice constant increases almost linearly from 8.1992 to 8.2260 Å with increasing calcination temperature from 250 to 800 °C. It is speculated that the value of the average oxidation state of manganese in the spinel phase is closely related to the lattice constant of the cubic unit cell. A lower calcination temperature results in a more oxidized manganese cation because manganese ions are stable preferentially as Mn^{4+} at lower temperatures.[22] For example, MnO_2 with all Mn^{4+} transforms progressively into Mn_2O_3 with all Mn^{3+} for the binary manganese oxide system as the temperature increases. The atomic radius of Mn^{4+} (0.67 Å) is smaller than that of Mn^{3+} (0.72 Å) and thus the lattice constant of the cubic unit cell of the spinel $LiMn_2O_4$ calcined at higher temperatures is larger than that of the spinel $LiMn_2O_4$ calcined at lower temperatures. The lattice constant of $LiMn_{1.95}Ni_{0.05}O_4$ powders calcined at 800 °C is 8.2236 Å which is in agreement with the literature value of 8.228 Å for $LiNi_{0.04}Mn_{1.96}O_4$.[15] The substitution of manganese with divalent nickel increases the average oxidation state of manganese above 3.5 to keep electrical neutrality in the spinel structure and thus there are many Mn^{4+} cations, which decrease the lattice constant of the $LiMn_{1.95}Ni_{0.05}O_4$ host structure.

Fig. 3 shows scanning electron micrographs (SEM) of the powders prepared from the gel precursors having the molar ratio of glycine to metal ions of 1.0 : 1 as a function of temperature. The presence of loosely agglomerated spherical particles with average grain size 70 nm was observed from the powders calcined at 220 °C. For the powders calcined at 650 °C, the particle size increased to 100 nm. As calcination temperature was increased, growth kinetics were favored and thus agglomerated spherical particles changed to larger particulates. When the gel precursors were heated at 800 °C, the particle size increased to about 600 nm with a fairly narrow particle-size distribution.

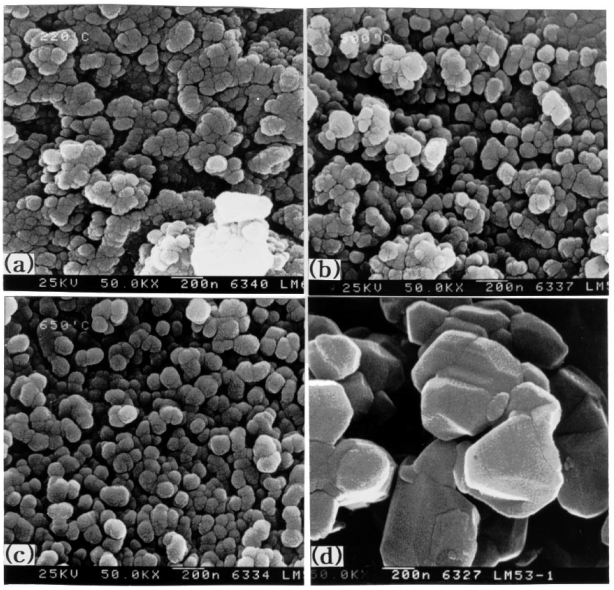

Fig. 3 Scanning electron micrographs of the $LiMn_2O_4$ powders calcined at (a) 220 °C, (b) 500 °C, (c) 650 °C, and (d) 800 °C.

Fig. 4 shows the X-ray diffraction patterns for the $LiMn_2O_4$ powders prepared from gel precursors having the molar ratio of glycine to metal ions of 0.5 and 1.5:1. Both the $LiMn_2O_4$ powders were calcined at 250 and 400 °C for 10 h in air. Whereas the X-ray diffraction pattern for the powders prepared by the molar ratio of glycine to metal ions of 1.5:1 and calcined at 250 °C presents no diffraction peaks indicating an amorphous phase, the powders prepared by the molar ratio of glycine to metal ions of 0.5:1 and calcined at 250 °C shows impurity phases such as β-MnO_2, Mn_2O_3, and Li_2CO_3 apart from the $LiMn_2O_4$ spinel phase. For the powders prepared by the molar ratio of glycine to metal ions of 0.5:1 and calcined at 400 °C, Mn_2O_3 peaks were still observed, though the proportion of the $LiMn_2O_4$ spinel phase is increased. On the contrary, the gel precursors prepared by the molar ratio of glycine to metal ions of 1.5:1 and calcined at 400 °C crystallized into a phase-pure $LiMn_2O_4$ spinel phase without any development of impurity phases.

Fig. 5 demonstrates the X-ray diffraction patterns for the powders prepared by the molar ratio of glycine to metal ions of 1.0, 1.5, 2.0, and 2.5:1 calcined at 700 °C for 10 h in air. It was confirmed from the XRD patterns that the spinel phase

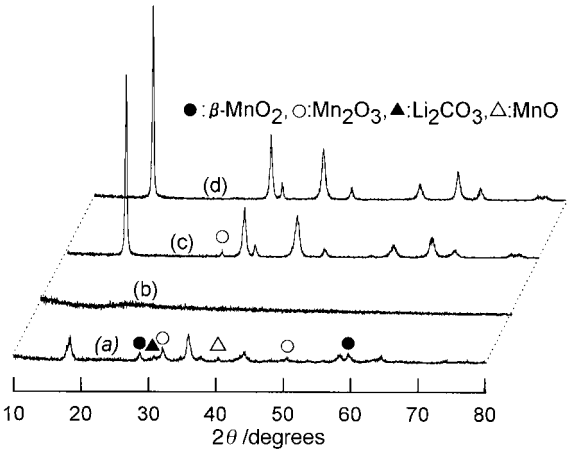

Fig. 4 X-Ray diffraction patterns of the $LiMn_2O_4$ powders prepared from the gel precursors having the molar ratio of glycine to metal ions of (a) 0.5:1 and calcined at 250 °C, (b) 1.5:1 and calcined at 250 °C, (c) 1.5:1 and calcined at 400 °C, and (d) 1.5:1 and calcined at 400 °C for 10 h in air.

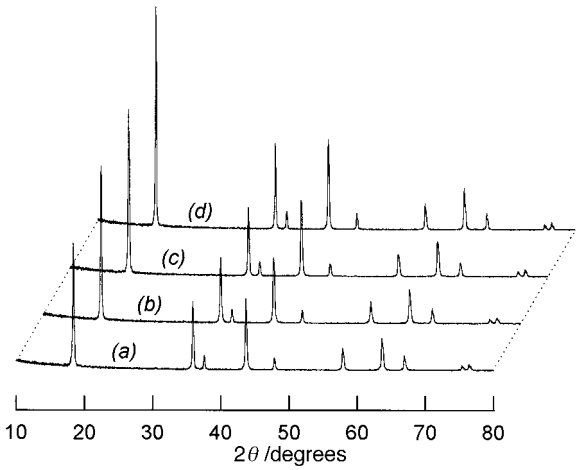

Fig. 5 X-Ray diffraction patterns of the $LiMn_2O_4$ powders prepared from the gel precursors having various molar ratios of glycine to total metal ions and calcined at 700 °C; (a) 1.0, (b) 1.5, (c) 2.0, and (d) 2.5:1.

could be formed regardless of the molar ratio of glycine to total metal ions tested. A close look at Fig. 5 reveals that the diffraction peaks are sharper and that their intensity is increased with increasing glycine quantity, which indicates an increase in the crystallinity of the spinel phase. In order to investigate the structural differences in the spinel phase at the various molar ratios of glycine to total metal ions, the Rietveld refinement was performed on the XRD data to obtain lattice constants. Fig. 6 shows the effect of the molar ratio of glycine to total metal ions on the lattice constant of the same powders as shown in Fig. 5. With increasing glycine quantity the lattice constant and thus the crystallinity of the $LiMn_2O_4$ powders increases linearly, although the extent of increase is not as much as the case of increasing calcination temperature as shown in Fig. 1.

In order to investigate the morphological features of the $LiMn_2O_4$ powders having different molar ratio of glycine to total metal ions, scanning electron microscopy (SEM) was used for the powders prepared from the gel precursors having molar ratios of glycine to metal ions of 0.5 and 2.0:1, and calcined at 700 °C for 10 h in air as shown in Fig. 7. The surface of the powders with a molar ratio of glycine to total metal ions of 0.5:1 contained monodispersed spherical fine particulates with an average particle size of about 200 nm. For the powders with a molar ratio of glycine to total metal ions

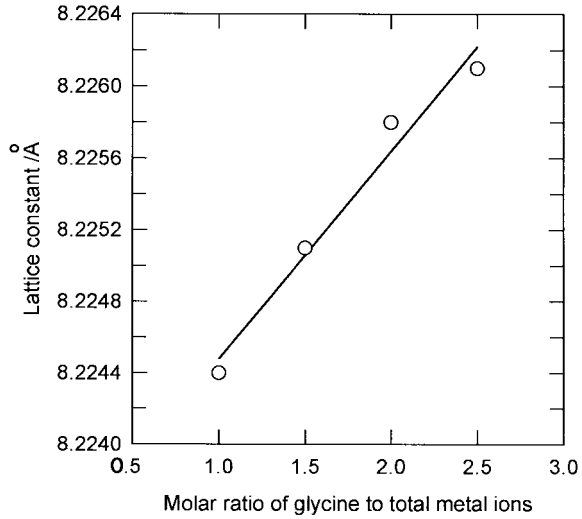

Fig. 6 Effect of the molar ratio of glycine to total metal ions on the lattice constant of the $LiMn_2O_4$ powders calcined at 700 °C for 10 h in air.

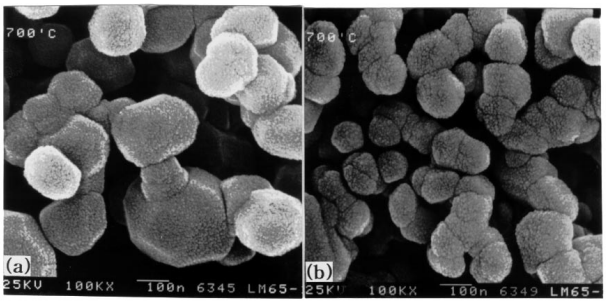

Fig. 7 Scanning electron micrographs of the $LiMn_2O_4$ powders calcined at 700 °C when the molar ratio of glycine to metal ions was (a) 0.5 and (b) 2.0:1.

of 2.0:1, it was observed that the particle size of the powders was 100 nm. The particle size of the former was two times smaller than that of the latter at the same calcination temperature.

Increase of the crystallinity and decrease of the particle size of the $LiMn_2O_4$ powders with the quantity of glycine used in preparing gel precursors can be explained as follows; the less glycine used in preparing gel precursors, the shorter is the distance between the Li and Mn cations, and thus the higher is the probability of crystallization between the cations. However, the amount of heterogeneously distributed cations in the calcined powders increased as shown in Fig. 4. Therefore, bigger particles with a low crystallinity are produced at lower glycine quantity. On the contrary, when the quantity of glycine is increased, the highly cross-linked gel precursors suppress the cation mobility and effectively prevent the cations from contacting each other. Thus, the degree of segregation of the cations occurring during calcination is decreased, and the homogeneously distributed cations crystallize into the spinel phase. It has been reported that the combustion heat from the chelating agents increases the crystallinity of the particles, yielding fluffy $LiMn_2O_4$ powders which result from large void volumes generated by CO and CO_2 during the combustion of the chelating agent.[8,16] This can be supported by the observation that the materials become more 'puffed up' after calcination in the presence of larger amounts of glycine at the same calcination temperature, which results in a decrease in the particle size of the $LiMn_2O_4$ powders. Therefore, it can be concluded that the amount of glycine determines the crystallinity and particle size of the $LiMn_2O_4$ powders.

Fig. 8 represents the specific discharge capacity of the Li/polymer electrolyte/$LiMn_{1.95}Ni_{0.05}O_4$ cell at the current densities of 0.15–2.0 mA cm^{-2}. In this cell, the composite cathode was prepared from the $LiMn_{1.95}Ni_{0.05}O_4$ powders calcined at 800 °C. The discharge capacity of the cell decreased very slowly with an increase in current density. For example, the cell delivered a capacity of 126, 122, and 116 mA h g^{-1} at current densities of 0.15, 0.5, and 1 mA cm^{-2} respectively. The cell showed an attractive capacity of 105 mA h g^{-1} at 1.5 mA cm^{-2} or 1.7 *C* rate. However, the discharge capacity of the cell abruptly decreased to 57 mA h g^{-1} at a current density of 2 mA cm^{-2} or 2.2 *C* rate. This may be due to the low conductivity of the polymer electrolyte compared to the liquid electrolyte. When the current densities were lowered to 0.15, 0.5, and 1.0 mA cm^{-2} at the 61, 71, 81st cycle, respectively, the discharge capacities increased to the original value. The observed cycling stability of the spinel $LiMn_{1.95}Ni_{0.05}O_4$ could be due to a small structural transition in the powders, and good contacts among the composite cathode constituents.

Fig. 9(a) and (b) show the charge/discharge curves with the number of cycles for the Li/polymer electrolyte/$LiMn_2O_4$ and $LiMn_{1.95}Ni_{0.05}O_4$ cells using the $LiMn_2O_4$ and $LiMn_{1.95}Ni_{0.05}O_4$ powders calcined at 800 °C. The Li/polymer electrolyte/$LiMn_2O_4$ cell showed two-stage reduction and oxidation processes which are characteristic of the manganese oxide spinel structure.[23,24] For the Li/polymer electrolyte/$LiMn_{1.95}Ni_{0.05}O_4$ cell, the two-stage reduction and oxidation processes became less distinct. This behavior suggests that the

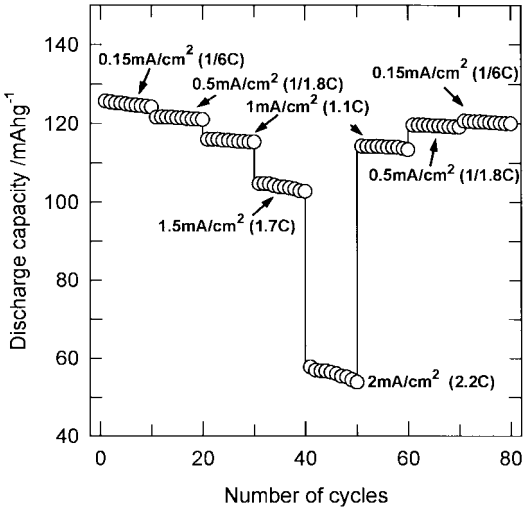

Fig. 8 Variation of specific discharge capacity with number of cycles at various discharge current densities of the Li/polymer electrolyte/$LiMn_{1.95}Ni_{0.05}O_4$ cell.

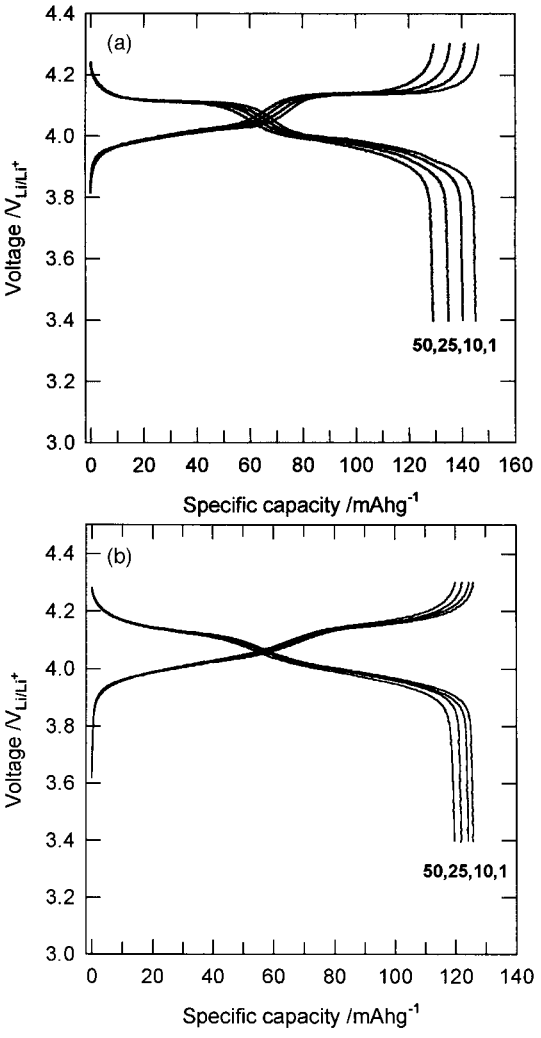

Fig. 9 Cycling charge/discharge curves with the number of cycles of (a) the Li/polymer electrolyte/$LiMn_2O_4$ and (b) the $LiMn_{1.95}Ni_{0.05}O_4$ cells.

local distortion of the host structure resulting from the substitution of nickel ions may eliminate the small Li–Li repulsion energy difference between the half-filled 8a sites in $Li_{0.5}Mn_2O_4$ and the completely filled sites in $LiMn_2O_4$.

Fig. 10 demonstrates the variation of discharge capacity with the number of cycles for the Li/polymer electrolyte/$LiMn_2O_4$ and $LiMn_{1.95}Ni_{0.05}O_4$ cells. The initial capacity of the $LiMn_2O_4$ electrode delivered 145 mA h g^{-1}. To our best knowledge, this is the highest value that has ever been reported in practice. The capacity slowly decreases with cycling and remained at 129 mA h g^{-1} at the 50th cycle. The discharge capacity of the $LiMn_{1.95}Ni_{0.05}O_4$ electrode decreased more slowly with cycling and remained at 120 mA h g^{-1} at the 50th cycle. This suggests that the theoretical capacity fading of the Ni-doped spinel phases is attributed to a decrease in the amount of Mn^{3+}, because the deintercalation of Li^+ from the spinel structure must be electrically compensated for by the oxidation of Mn^{3+} to Mn^{4+} and thus, the capacity of the $LiMn_{1.95}Ni_{0.05}O_4$ electrode was lower than that of the $LiMn_2O_4$ one. The cycling stability of the Ni-doped spinel compared to the stoichiometric $LiMn_2O_4$ was due to the suppression of the Jahn–Teller distortion in the spinel electrode at the end of discharge since the M–O bonds for M = Ni, Co, or Cr are stronger than the Mn–O bond.[9] Therefore, the Ni dopant could enhance the stability of the octahedral sites in the spinel host structure. It should also be noted from Fig. 2 that the lattice constant of the Ni-doped spinel is smaller than that of the standard $LiMn_2O_4$. Another factor of the cycling stability of the Ni-doped spinel is attributed to the volume changes during the intercalation and deintercalation reaction of lithium ions, which will be less than those of the stoichiometric $LiMn_2O_4$.

In order to investigate the capacity fading of Li/polymer electrolyte/$LiMn_{1.95}Ni_{0.05}O_4$ cell with cycling, ac impedence spectra with respect to the number of cycles were measured. Fig. 11 illustrates typical Nyquist plots obtained from the Li/polymer electrolyte/$LiMn_{1.95}Ni_{0.05}O_4$ cell in a fully charged state with respect to the number of cycles. The impedance spectra consist of one semicircle in the high and intermediate frequency range, a line inclined at a constant angle to the real axis in the low frequency range of 5 Hz to 10 mHz, and a capacitive line due to the accumulation of lithium ions at the center of the oxide particle in the frequency range below 10 mHz. The semicircle in the higher frequency range is related to the reactions at the interface of the polymer electrolyte/electrode (Li and oxide electrode) and the inclined line in the lower frequency range is due to Warburg impedance which

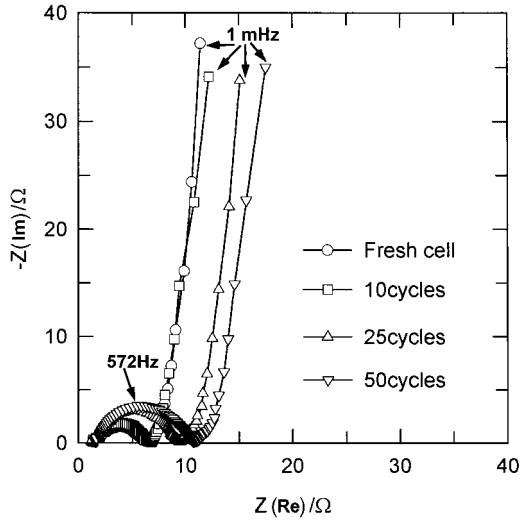

Fig. 11 Ac impedance spectra of the Li/polymer electrolyte/$LiMn_{1.95}Ni_{0.05}O_4$ cell in fully charged state as a function of number of cycles.

is associated with lithium ion diffusion through the $LiMn_{1.95}Ni_{0.05}O_4$ particle.[24] The high-frequency semicircle is progressively increased with the increase in number of cycles which indicates an increased interfacial resistance between polymer electrolyte and electrode (Li and oxide electrode). The apparent chemical diffusivity of lithium ions in the porous $LiMn_2O_4$ and $LiMn_{1.95}Ni_{0.05}O_4$ electrodes with respect to the number of cycles was calculated using the relation (1)[25]

$$\tilde{D}_{Li^+} = \frac{\pi f_T r^2}{1.94} \quad (1)$$

where f_T is the frequency at which the impedance spectrum shows a transition from semi-infinite diffusion behavior to finite-length diffusion behavior. The average radius r of the oxide was determined from scanning electron microscopic observation.

The calculated chemical diffusivities of lithium ions in the $LiMn_2O_4$ and $LiMn_{1.95}Ni_{0.05}O_4$ electrodes are plotted against number of cycles in Fig. 12. The chemical diffusivities were determined to be of orders of 10^{-10} to 10^{-11} cm^2 s^{-1}. The chemical diffusivity within both electrodes decreases with increasing number of cycles. However, it should be noted that

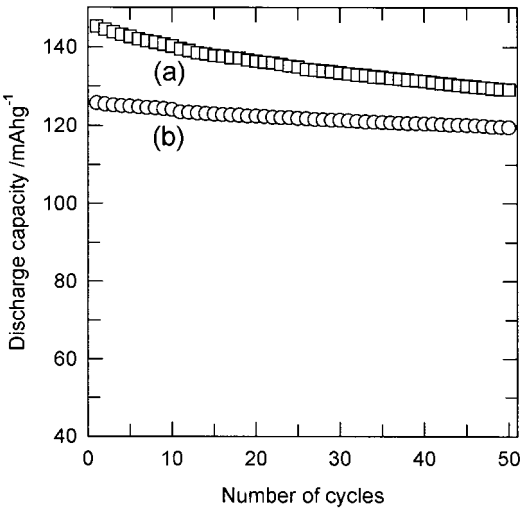

Fig. 10 Variation of discharge capacity with the number of cycles of (a) Li/polymer electrolyte/$LiMn_2O_4$ and (b) Li/polymer electrolyte/$LiMn_{1.95}Ni_{0.05}O_4$ cells.

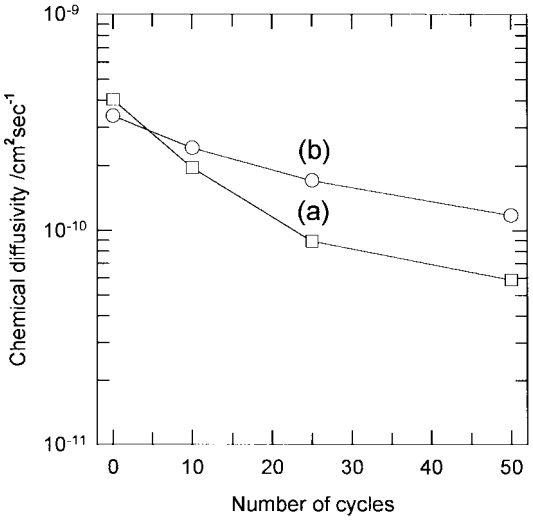

Fig. 12 Variation of chemical diffusivity of the porous (a) $LiMn_2O_4$ and (b) $LiMn_{2.95}Ni_{0.05}O_4$ electrodes as a function of the number of cycles.

the chemical diffusivity of lithium ions markedly decreases with cycling for the $LiMn_2O_4$ electrode. It is speculated that the decrease in chemical diffusivity could be attributed to the decreased number of vacant sites available for the diffusion of lithium ions which resulted from volume change and Jahn–Teller distortion of the spinel host structure. Liu *et al.* reported that the $LiMn_2O_4$ powders after 80 cycles had a tetragonal phase, which suggests the onset of the Jahn–Teller effect causes a severe structural distortion, leading to a decrease in vacant sites.[12] The capacity fading of the $LiMn_2O_4$ and $LiMn_{1.95}Ni_{0.05}O_4$ electrodes appears to be related to the decrease in chemical diffusivity as well as the increase in interfacial resistance between polymer electrolyte and electrode (Li and oxide electrode). The good capacity retention for the $LiMn_{1.95}Ni_{0.05}O_4$ electrode compared to the stoichiometric $LiMn_2O_4$ is attributed to the suppression of the Jahn–Teller distortion, smaller volume change of the unit-cell (smaller lattice constant) and higher chemical diffusivity in the $LiMn_{1.95}Ni_{0.05}O_4$ electrode as mentioned above.

Conclusions

The spinel $LiMn_2O_4$ powders with submicron, monodispersed, and highly homogeneous particles were synthesized by a sol–gel method using an aqueous solution of metal acetate containing glycine as a chelating agent. While the crystallinity and lattice constant of the $LiMn_2O_4$ powders were increased, the particle size of the $LiMn_2O_4$ powders was decreased with an increase in glycine quantity. Polycrystalline $LiMn_2O_4$ powders calcined at 250–800 °C were found to be composed of very uniformly sized particulates with an average particle size of 70–600 nm depending on the processing conditions. The initial capacity of the cell with the $LiMn_{1.95}Ni_{0.05}O_4$ was lower than the cell with the stoichiometric $LiMn_2O_4$, but the cycle performance was improved at the expense of capacity. The good capacity retention of the $LiMn_{1.95}Ni_{0.05}O_4$ electrode compared to the stoichiometric $LiMn_2O_4$ is attributed to the suppression of the Jahn–Teller distortion, smaller volume change of the unit-cell and higher chemical diffusivity of lithium ions.

References

1 T. Ohuzuka, M. Kitagawa and T. Hirai, *J. Electrochem. Soc.*, 1990, **137**, 760.
2 D. Guyomard and J. M. Tarascon, *Solid State Ionics*, 1994, **69**, 222.
3 R. J. Gummow, A. de Kock and M. M. Thackeray, *Solid State Ionics*, 1994, **69**, 59.
4 D. H. Jang, Y. J. Shin and S. M. Oh, *J. Electrochem. Soc.*, 1996, **143**, 2204.
5 Y. Xia, Y. Zhou and M. Yoshio, *J. Electrochem. Soc.*, 1997, **144**, 2593.
6 D. Guyomard and J. M. Tarascon, *Solid State Ionics*, 1994, **69**, 222.
7 X. Qiu, X. Sun, W. Shen and N. Chen, *Solid State Ionics*, 1997, **93**, 335.
8 Y.-K. Sun, *Solid State Ionics*, 1997, **100**, 115.
9 Li Guohua, H. Ikuta, T. Uchida and M. Wakihara, *J. Electrochem. Soc.*, 1996, **143**, 178.
10 R. Bittihn, R. Herr and D. Hoge, *J. Power Sources*, 1993, **43–44**, 223.
11 G. Pistoia and G. Wang, *Solid State Ionics*, 1993, **66**, 135.
12 W. Liu, K. Kowal and G. C. Farrington, *J. Electrochem. Soc.*, 1997, **143**, 3590.
13 A. D. Robertson, S. H. Lu, W. F. Averill and W. F. Howard, Jr., *J. Electrochem. Soc.*, 1997, **144**, 3500.
14 T. Tsumura, A. Shimizu and M. Inagaki, *J. Mater. Chem.*, 1993, **3**, 995.
15 W. Liu, G. C. Farrington, F. Chaput and B. Dunn, *J. Electrochem. Soc.*, 1996, **143**, 87.
16 Y.-K. Sun, I.-H. Oh and K. W. Kim, *Ind. Eng. Chem. Res.*, 1997, **36**, 4839.
17 A. Hooper and B. C. Tofield, *J. Power Sources*, 1984, **11**, 33.
18 B. C. H. Steele, G. E. Lagos, P. C. Spurdens, C. Forsyth and A. D. Foord, *Solid State Ionics*, 1983, **9** and **10**, 391.
19 P. G. Bruce and F. Krok, *Solid State Ionics*, 1989, **36**, 171.
20 B. V. Ratnakumar, S. DiStefano and C. P. Bankston, *J. Appl. Electrochem.*, 1989, **19**, 813.
21 R. Koksbang, I. I. Olsen, P. E. Tonder, N. Knudsen and D. Fauteux, *J. Appl. Electrochem.*, 1991, **21**, 301.
22 C. Masquelier, M. Tabuchi, K. Ado, R. Kanno, Y. Kobayashi, Y. Maki, O. Nakamura and J. B. Goodenough, *J. Solid State Chem.*, 1996, **123**, 255.
23 M. M. Thackery, W. I. F. David, P. G. Bruce and J. B. Goodenough, *Mater. Res. Bull.*, 1983, **18**, 461.
24 Y.-M. Choi and S.-I. Pyun, *Solid State Ionics*, 1997, **99**, 173.
25 B. E. Conway, *J. Electrochem. Soc.*, 1991, **138**, 1569.

Paper 8/04483J